

## Probing the High Momentum Component of the Deuteron at High $Q^2$

W. U. Boeglin,<sup>1</sup> L. Coman,<sup>1</sup> P. Ambrozewicz,<sup>1</sup> K. Aniol,<sup>2</sup> J. Arrington,<sup>3</sup> G. Batigne,<sup>4</sup> P. Bosted,<sup>5</sup> A. Camsonne,<sup>5</sup> G. Chang,<sup>6</sup> J. P. Chen,<sup>5</sup> S. Choi,<sup>7</sup> A. Deur,<sup>5</sup> M. Epstein,<sup>2</sup> J. M. Finn,<sup>8,\*</sup> S. Frullani,<sup>9</sup> C. Furget,<sup>4</sup> F. Garibaldi,<sup>9</sup> O. Gayou,<sup>10,5</sup> R. Gilman,<sup>10,5</sup> O. Hansen,<sup>5</sup> D. Hayes,<sup>11</sup> D. W. Higinbotham,<sup>5</sup> W. Hinton,<sup>11</sup> C. Hyde,<sup>11</sup> H. Ibrahim,<sup>12,11</sup> C. W. de Jager,<sup>5</sup> X. Jiang,<sup>10</sup> M. K. Jones,<sup>5</sup> L. J. Kaufman,<sup>13,†</sup> A. Klein,<sup>14</sup> S. Kox,<sup>4</sup> L. Kramer,<sup>1</sup> G. Kumbartzki,<sup>10</sup> J. M. Laget,<sup>5</sup> J. LeRose,<sup>5</sup> R. Lindgren,<sup>15</sup> D. J. Margaziotis,<sup>2</sup> P. Markowitz,<sup>1</sup> K. McCormick,<sup>16</sup> Z. Meziani,<sup>7</sup> R. Michaels,<sup>5</sup> B. Milbrath,<sup>5</sup> J. Mitchell,<sup>5,‡</sup> P. Monaghan,<sup>17</sup> M. Moteabbed,<sup>1</sup> P. Moussiegt,<sup>4</sup> R. Nasseripour,<sup>1</sup> K. Paschke,<sup>15</sup> C. Perdrisat,<sup>8</sup> E. Piassetzky,<sup>18</sup> V. Punjabi,<sup>19</sup> I. A. Qattan,<sup>20,3</sup> G. Quémener,<sup>4</sup> R. D. Ransome,<sup>10</sup> B. Raue,<sup>1</sup> J. S. Réal,<sup>4</sup> J. Reinhold,<sup>1</sup> B. Reitz,<sup>5</sup> R. Roché,<sup>21</sup> M. Roedelbronn,<sup>22</sup> A. Saha,<sup>5,\*</sup> K. Slifer,<sup>23</sup> P. Solvignon,<sup>3</sup> V. Sulkosky,<sup>5,§</sup> P. E. Ulmer,<sup>11,‡</sup> E. Voutier,<sup>4</sup> L. B. Weinstein,<sup>11</sup> B. Wojtsekhowski,<sup>5</sup> and M. Zeier<sup>15</sup>

(For the Hall A Collaboration)

<sup>1</sup>Florida International University, University Park, Florida 33199, USA

<sup>2</sup>California State University, Los Angeles, Los Angeles, California 90032, USA

<sup>3</sup>Argonne National Laboratory, Argonne, Illinois 60439, USA

<sup>4</sup>LPSC, Université Joseph Fourier, CNRS/IN2P3, INPG, Grenoble, France

<sup>5</sup>Thomas Jefferson National Accelerator Facility, Newport News, Virginia 23606, USA

<sup>6</sup>University of Maryland, College Park, Maryland 20742, USA

<sup>7</sup>Temple University, Philadelphia, Pennsylvania 19122, USA

<sup>8</sup>College of William and Mary, Williamsburg, Virginia 23187, USA

<sup>9</sup>INFN, Sezione Sanita and Istituto Superiore di Sanita, Laboratorio di Fisica, I-00161 Rome, Italy

<sup>10</sup>Rutgers, The State University of New Jersey, Piscataway, New Jersey 08854, USA

<sup>11</sup>Old Dominion University, Norfolk, Virginia 23529, USA

<sup>12</sup>Physics Department, Faculty of Science, Cairo University, Giza 12613, Egypt

<sup>13</sup>University of Massachusetts Amherst, Amherst, Massachusetts 01003, USA

<sup>14</sup>Los Alamos National Laboratory, Los Alamos, New Mexico 87545, USA

<sup>15</sup>University of Virginia, Charlottesville, Virginia 22901, USA

<sup>16</sup>Kent State University, Kent, Ohio 44242, USA

<sup>17</sup>Hampton University, Hampton, Virginia 23668, USA

<sup>18</sup>University of Tel Aviv, Tel Aviv 69978, Israel

<sup>19</sup>Norfolk State University, Norfolk, Virginia 23504, USA

<sup>20</sup>Department of Physics, Khalifa University of Science, Technology, and Research, Sharjah, United Arab Emirates

<sup>21</sup>Ohio University, Athens, Ohio 45701, USA

<sup>22</sup>University of Illinois, Urbana Champaign, Illinois 61820, USA

<sup>23</sup>The University of New Hampshire, Durham, New Hampshire 03824, USA

(Received 22 July 2011; published 19 December 2011)

The  ${}^2\text{H}(e, e'p)n$  cross section at a momentum transfer of  $3.5 \text{ (GeV}/c)^2$  was measured over a kinematical range that made it possible to study this reaction for a set of fixed missing momenta as a function of the neutron recoil angle  $\theta_{\text{nq}}$  and to extract missing momentum distributions for fixed values of  $\theta_{\text{nq}}$  up to  $0.55 \text{ GeV}/c$ . In the region of  $35^\circ \leq \theta_{\text{nq}} \leq 45^\circ$  recent calculations, which predict that final-state interactions are small, agree reasonably well with the experimental data. Therefore, these experimental reduced cross sections provide direct access to the high momentum component of the deuteron momentum distribution in exclusive deuteron electrodisintegration.

DOI: 10.1103/PhysRevLett.107.262501

PACS numbers: 25.30.Fj, 25.60.Gc

The understanding of the short-range structure of the deuteron is of fundamental importance for the advancement of our understanding of nuclear matter at small distances. To probe the short-range properties of the deuteron, one has to investigate configurations where the two nucleons come very close together and are strongly overlapping. The basic problem is to what extent these configurations can be

described simply in terms of two nucleons with high initial relative momenta. The ultimate quantity to be investigated in this case is the high momentum component of the deuteron wave function. Traditionally, three classes of reactions are used to study the high momentum part of the deuteron wave function: elastic scattering and inclusive and exclusive electrodisintegration reactions.

Elastic electron-deuteron scattering probes the integrated characteristics of the wave function via the deuteron form factors. At large four-momentum transfer,  $-Q^2$ , the scattering becomes sensitive to the high momentum component of the deuteron wave function. The analysis of experimental data [1] showed that, at presently available energies, it is practically impossible to discriminate between different theoretical approaches [2,3] used to calculate the deuteron elastic form factor  $A(Q^2)$ . One needs additional constraints on the deuteron wave function at short distances.

Inclusive, quasielastic ( $e, e'$ ) reactions provide another way of probing high momentum components of the deuteron, especially at high  $Q^2$  and in the  $x_B \geq 1$  region [4–6], where  $x_B = Q^2/2M\nu$  (with  $M$  as the nucleon mass and  $\nu$  as the energy of the virtual photon) is the Bjorken scaling variable. In this regime, the cross section depends on an integral of the deuteron momentum distribution, with the longitudinal nucleon momentum component (with respect to the virtual photon momentum  $\vec{q}$ ) as the lower limit. However, the difficulties of ensuring small contributions from inelastic processes (growing with  $Q^2$ ) and final-state interactions (FSIs) at large  $x_B$  (see, e.g., [7,8]) reduce the sensitivity to the deuteron wave function at short internucleon distances, although the high momentum component is certainly important in this kinematics.

The most direct way of studying high nucleon momenta is to investigate the quasielastic electrodisintegration of the deuteron via the  ${}^2\text{H}(e, e'p)n$  reaction at high missing momenta (the momentum of the recoiling neutron)  $\vec{p}_m = \vec{q} - \vec{p}_f$ , where  $\vec{p}_f$  is the momentum of the outgoing, observed proton. Within the plane wave impulse approximation (PWIA),  $-\vec{p}_m$  corresponds to the initial momentum of the target nucleon before the interaction. Thus, the strategy in these studies is to probe the cross section at  $p_m$  values as large as possible. However, depending on the selected kinematics, these studies can be overwhelmed by FSIs where the outgoing proton interacts with the recoiling neutron, or by processes where the virtual photon couples to the exchanged meson (MEC) or where the nucleon is excited to an intermediate  $\Delta$  state (IC). The dominance of FSI, MEC, and IC has seriously affected previous experiments at  $Q^2 < 1$  (GeV/c)<sup>2</sup> [9–13] leading to the overall conclusion that these experiments do not provide good constraints on the high momentum components of the deuteron wave function.

The condition  $Q^2 \geq 1$  (GeV/c)<sup>2</sup> is necessary in order to enhance contributions of reaction mechanisms which probe the short-range structure of the deuteron and to suppress competing long-range processes for the following reasons: (i) the MEC contribution should be suppressed by an additional factor of  $(1 + Q^2/\Lambda)^{-4}$  with  $\Lambda = 0.8 - 1$  (GeV/c)<sup>2</sup>, as compared to the quasielastic contribution [14,15]; (ii) the large  $Q^2$  limit should allow one to probe the wave function in the  $x > 1$  region which is

far from the inelastic threshold, thereby suppressing IC contributions; and (iii) final-state interactions of the outgoing nucleon should follow the eikonal dynamics, with a strong angular anisotropy dominating mainly in transverse directions. This situation generated a multitude of theoretical studies of the  ${}^2\text{H}(e, e'p)n$  reaction in the high  $Q^2$  regime [14,16–26]. The PWIA results of calculations described in Refs. [14,18,21,24,26] differ at larger  $p_m$  due to differences in the wave functions and in details of the off-shell electron nucleon interaction used, but all predict small FSI contributions (10–20%) for  $35^\circ \leq \theta_{\text{ng}} \leq 45^\circ$ .

We report new  ${}^2\text{H}(e, e'p)n$  cross sections measured at high momentum transfer for well-defined kinematic settings. The wide range in missing momenta and neutron recoil angles allows one for the first time to access the high momentum components of the deuteron momentum distribution and probe the validity of current models of the reaction dynamics. The kinematic region covered overlaps with a recent  ${}^2\text{H}(e, e'p)n$  experiment performed using the CEBAF Large Acceptance Spectrometer (CLAS) at Jefferson Lab [27], which concluded that FSI and IC are dominating the momentum distribution except for  $p_m < 0.1$  GeV/c or  $\theta_{\text{ng}} > 110^\circ$ . However, to obtain reasonable statistical precision, the data were integrated over the full  $\theta_{\text{ng}}$  range for the momentum distributions and over a large  $p_m$  range for the angular distributions, in contrast to the data presented below.

At a fixed  $Q^2 = 3.5$  (GeV/c)<sup>2</sup>, the  ${}^2\text{H}(e, e'p)n$  cross section was measured for specific missing momenta  $p_m = 0.1, 0.2, 0.4, 0.5$  GeV/c, while the angle  $\theta_{\text{ng}}$  of the recoiling neutron with respect to  $\vec{q}$  was varied.  $\theta_{\text{ng}}$  is also referred to hereafter as the recoil angle. For  $p_m = 0.4, 0.5$  GeV/c, the largest recoil angles accessible were limited by the maximum momentum that the proton spectrometer was able to detect (3.1 GeV/c). Keeping  $p_m$  and  $Q^2$  constant required the energy transfer, the electron scattering angle, the proton final momentum, and the proton direction to be adjusted accordingly for each value of  $\theta_{\text{ng}}$ . As the energy transfer and recoil angle changed,  $x_B$  changed as well between 0.78 and 1.52, with large  $x_B$  values corresponding to small recoil angles.

The experiment was carried out using the two high-resolution spectrometers in Hall A at Jefferson Lab at an electron beam momentum of 5.008 GeV/c. The left arm detected the electrons and the right arm the ejected protons. The deuterium target consisted of a 15 cm long cylinder filled with liquid deuterium and was part of the Hall A cryogenic target system [28]. An identical target cell filled with liquid hydrogen was used for calibration and to determine the coincidence efficiency. The electron beam was rastered over an area of  $2 \times 2$  mm<sup>2</sup>, and the liquids were continuously circulated in order to minimize density variations due to boiling. We found a typical reduction of the effective deuteron target thickness due to boiling by a factor of  $0.94 \pm 0.02$  for an average current of 100  $\mu\text{A}$ . The

cross sections were corrected for detector inefficiencies on a run-by-run basis and for an overall coincidence efficiency, determined from the measured  $^1\text{H}(e, e')$  elastic cross section, which was found to be  $96.4 \pm 2$  percent of the published value from the fit of Table I in Ref. [29]. The systematic error due to uncertainties in the measured kinematic variables was calculated for each data bin and added quadratically to the statistical error. An overall error of 4.5% was added to take into account errors in beam energy, beam charge measurements, detector efficiencies, target thickness, and target boiling corrections.

The spectrometer detection systems in the two arms were very similar: vertical drift chambers were used for tracking, and two scintillation counter planes ( $S1/S2$ ) following the vertical drift chambers provided timing and trigger signals. In addition, the electron arm was equipped with a gas Čerenkov detector for electron/ $\pi^-$  discrimination. We found that the gas Čerenkov detector was sufficient for the  $\pi^-$  rejection in this experiment. At this large momentum transfer and at the large  $x_B$  kinematics, the  $\pi^-$  background was not a concern. A detailed description of the spectrometer systems and the target system can be found in Ref. [28]. The momentum acceptance used for both spectrometers was set by software to  $\delta = \Delta p/p_0 = \pm 4\%$ , where  $p_0$  is the central momentum of the spectrometer.

The solid angle of each spectrometer was defined by software cuts at the entrance of the first quadrupole magnet. In addition, a second, global cut on the multidimensional acceptance of each spectrometer was applied by means of  $R$  functions [30]. The phase space acceptance was calculated using the Hall A Monte Carlo code MCEEP [31]. The extracted cross sections were radiatively corrected using the Monte Carlo code SIMC [32,33], where the yield was estimated with a theoretical calculation by J. M. Laget [24] that included final-state interactions and reproduced the experimental yield quite well.

Several spectrometer settings contributed to a full angular distribution, and the condition of constant  $Q^2$  and constant  $p_m$  was maintained for the central setting only. Within the phase space acceptance defined by the two spectrometers, the kinematic variables varied slightly around their central values as a function of the angle  $\theta_{\text{nq}}$ . This led to variations of the experimental cross section as a function of  $\theta_{\text{nq}}$  that were independent of reaction mechanism effects. In order to reduce these variations, the experimental cross section was divided by the PWIA cross section  $\sigma_{\text{PWIA}} = n_p(p_m)k\sigma_{\text{CC1}}$ , where  $k$  is a kinematic factor,  $n_p(p_m)$  refers to the Paris momentum distribution, and  $\sigma_{\text{CC1}}$  is the de Forest off-shell cross section [34] calculated using the form factor parametrization from Table I of Ref. [29]. Theoretical cross sections were calculated using the averaged kinematics determined for each bin in  $\theta_{\text{nq}}$ , included bin center corrections, and were divided by the same PWIA cross section as the experimental

ones. The resulting ratios  $R(\theta_{\text{nq}}) = \sigma_{\text{exp}}/\sigma_{\text{PWIA}}$  were then averaged for overlapping  $\theta_{\text{nq}}$  bins, and the resulting angular distributions are shown in Fig. 1.

The angular distribution shown in Fig. 1(a) for missing momentum  $p_m = 0.2 \pm 0.02$  GeV/ $c$  shows a clear reduction of  $R$  for  $\theta_{\text{nq}}$  around  $75^\circ$  ( $x_B \sim 1$ ). For missing momentum  $p_m = 0.4 \pm 0.02$  GeV/ $c$  [Fig. 1(b)] and  $p_m = 0.5 \pm 0.02$  GeV/ $c$  [Fig. 1(c)],  $R$  shows a peak at around  $75^\circ$  with a maximal value of  $\sim 1.6$  and  $\sim 2.5$ , respectively. The dependence of  $R$  on  $\theta_{\text{nq}}$  reflects the angular dependence of final-state interactions at high  $Q^2$  and is in agreement with the measurement of Ref. [27] for missing momenta  $0.4 \leq p_m \leq 0.6$  GeV/ $c$ .

The strong angular dependence indicates that the struck proton is energetic enough that its interaction with the

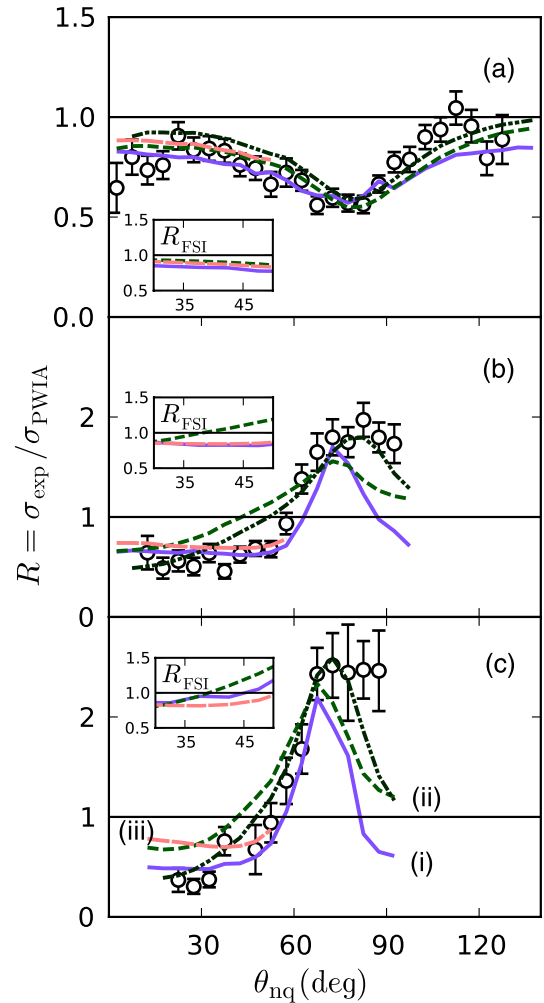


FIG. 1 (color online). The ratio  $R(\theta_{\text{nq}}) = \sigma_{\text{exp}}/\sigma_{\text{PWIA}}$ . (a)  $p_m = 0.2$  GeV/ $c$ , (b)  $p_m = 0.4$  GeV/ $c$ , and (c)  $p_m = 0.5$  GeV/ $c$ . (i) Solid (purple) lines denote MS [14,18,26] using the CD-Bonn potential; (ii) short-dashed (green) lines denote JML [24], while dashed–double-dotted (black) lines denote JML with MEC and IC; and (iii) long-dashed (pink) lines denote JVO [21]. Insets:  $R_{\text{FSI}} = \sigma_{\text{FSI}}/\sigma_{\text{PWIA}}^{\text{th}}$  for  $35^\circ \leq \theta_{\text{nq}} \leq 45^\circ$ .

recoiling, slow neutron is in the eikonal or geometric regime, where it is well-known that the slow particle recoils almost in a perpendicular direction with respect to the fast particle. As a consequence, there exist regions in recoil angles where FSIs contribute minimally to the cross section, allowing for increased sensitivity to the momentum distribution of the proton in the ground-state wave function. Note that, at low energies, the angular distribution of the rescattering process is considerably more isotropic, making it impossible to isolate regions with minimal FSI contribution.

Three different theoretical calculations were obtained: (1) a calculation by M. Sargsian [14,18,26], referred to as MS below, using the charge-dependent Bonn (CD-Bonn) or the Paris potentials; (2) cross sections from J. M. Laget's model [24], referred to as JML, using the Paris potential; and (3) results from the model of Jeschonnek and Van Orden [21], which will be labeled JVO below. The relativistically covariant calculation of JVO is currently limited to small recoil angles.

The model predictions of  $R = \sigma_{\text{calc}}/\sigma_{\text{PWIA}}$  are compared to experimental data in Fig. 1. For small missing momenta ( $p_m < 0.2 \text{ GeV}/c$ ) and  $\theta_{\text{nq}} < 30^\circ$ , all calculations agree with each other within 20%. For larger angles and especially larger missing momenta, deviations between the experiment and the calculations and between the different calculations themselves are considerably larger. For  $p_m = 0.4$  and  $0.5 \text{ GeV}/c$ , MS correctly describes the rise of  $R$  with  $\theta_{\text{nq}}$  but predicts a faster falloff after the maximum than is observed. JML predicts a considerably wider rescattering peak. Including MEC and  $\Delta$  excitation improves the agreement considerably at

$p_m = 0.4, 0.5 \text{ GeV}/c$  [Fig. 1(c)] but worsens the agreement for  $p_m = 0.2 \text{ GeV}/c$  [Fig. 1(a)]. The value of the maximum agrees with the experiment for both calculations. For  $p_m = 0.4, 0.5 \text{ GeV}/c$  and  $\theta_{\text{nq}} < 50^\circ$ , MS and JVO describe the data considerably better than JML, excluding MEC and  $\Delta$  contributions. The ratio  $R_{\text{FSI}} = \sigma_{\text{FSI}}/\sigma_{\text{PWIA}}^{\text{th}}$ , where  $\sigma_{\text{FSI}}$  is a calculated cross section including FSI and  $\sigma_{\text{PWIA}}^{\text{th}}$  is the corresponding PWIA cross section, demonstrates that all calculations show relatively small contributions of FSI for  $35^\circ < \theta_{\text{nq}} < 45^\circ$  (insets in Fig. 1). For  $0.2 \leq p_m \leq 0.5 \text{ GeV}/c$ , on average MS predicts between  $-18\%$  and  $-5\%$  FSI, JML between  $-9\%$  and  $+5\%$  FSI, and JVO between  $-12\%$  and  $-16\%$  FSI. This indicates a kinematic region where the cross section is dominated by PWIA and should therefore reflect directly the deuteron momentum distribution.

We extracted the  ${}^2\text{H}(e, e'p)n$  cross section for three sets of fixed angles  $\theta_{\text{nq}}$  with a bin width of  $\pm 5^\circ$ . For each of these three recoil angles, we determined the cross section as a function of missing momentum and calculated the reduced cross section  $\sigma_{\text{red}} = \sigma_{\text{exp}}/(k\sigma_{\text{CC1}})$  using the same form factor as previously (Table I in Ref. [29]). We included all spectrometer settings that contributed to the same  $(p_m, \theta_{\text{nq}})$  bin and determined the averaged, reduced cross section as well as the averaged kinematics. The theoretical cross sections have been treated the same way as the experimental ones. The resulting experimental momentum distributions are shown in Fig. 2.

The results for  $\theta_{\text{nq}} = 75^\circ$  [Fig. 2(c)] show a behavior of reduced  ${}^2\text{H}(e, e'p)n$  deuteron cross sections as a function of missing momentum typical to the situation in which the process is dominated by FSI. As the FSI

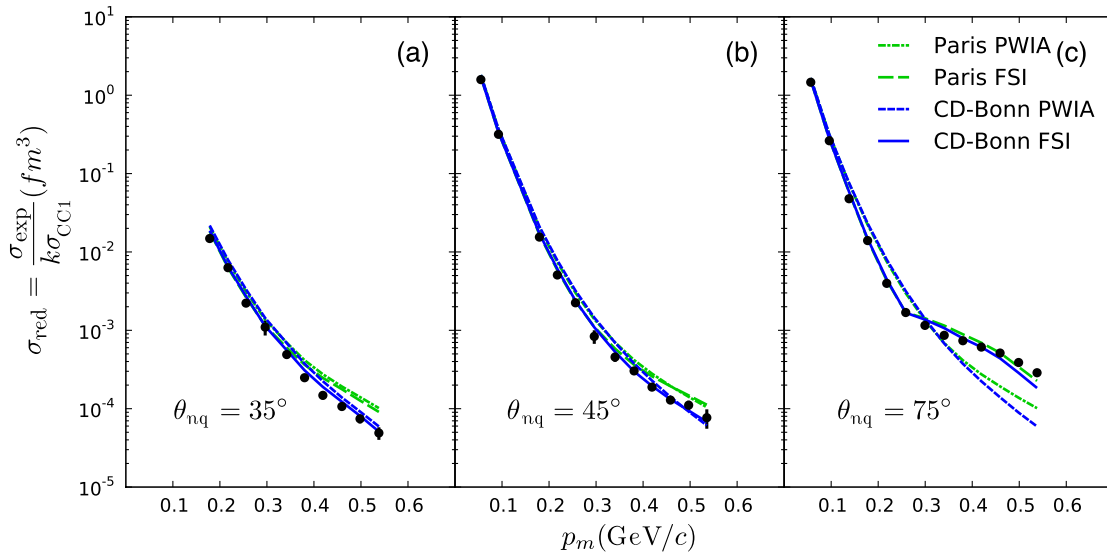


FIG. 2 (color online). The reduced cross section  $\sigma_{\text{red}}(p_m)$  as a function of missing momentum  $p_m$  is shown in (a)–(c) for  $\theta_{\text{nq}} = 35^\circ$ ,  $45^\circ$ , and  $75^\circ$ , respectively, with a bin width of  $\pm 5^\circ$ . CD-Bonn potential: short-dashed (blue) lines with PWIA, solid (blue) lines with FSI. Paris potential: dash-dotted (green) lines with PWIA, long-dashed (green) lines with FSI. The PWIA results are identical for all angles. All calculations are from the MS model [14,18,26].

contribution is dominated by smaller initial momenta of the struck proton than the observed  $p_m$ , the reduced cross section exhibits a “flattening” (smaller falloff with  $p_m$ ) for  $p_m > 0.3$  GeV/ $c$ . This flattening has been observed in all previous measurements in which the cross section was dominated by FSI, such as in Ref. [12], where the  ${}^2\text{H}(e, e'p)n$  cross section was measured at lower  $Q^2$  ( $\sim 0.6$  GeV $^2$ ) and  $x_B \sim 1$ , or as in Ref. [10], measured at much lower energies and  $x_B < 1$ , where, in addition to FSI, the cross section was dominated also by MEC and IC contributions.

In Fig. 2, the experimental reduced cross sections are compared to a calculation by M. Sargsian with wave functions from the CD-Bonn and the Paris potentials. For the CD-Bonn potential, the PWIA results are shown as short-dashed (blue) curves and the FSI results as solid (blue) lines. For the Paris potential, the PWIA results are shown as dash-dotted (green) curves and the FSI results as long-dashed (green) lines. Both calculations at  $\theta_{\text{ng}} = 75^\circ$  including FSI agree quite well with the measurement. The PWIA calculations cannot reproduce the data for  $p_m > 0.1$  GeV/ $c$ , and, for  $p_m > 0.45$  GeV/ $c$ , the two calculations increasingly deviate from each other.

Because of the observed, strong angular anisotropy of high energy FSI (Fig. 1), one can select recoil angles where FSIs are minimal. For example, in Figs. 2(a) and 2(b), at  $\theta_{\text{ng}} = 35^\circ$  and  $\theta_{\text{ng}} = 45^\circ$ , the reduced cross sections display a qualitatively different behavior as a function of  $p_m$ . The falloff is considerably steeper for  $p_m > 0.3$  GeV/ $c$  and follows closely the general shape of the deuteron wave function in momentum space, reflecting the diminishing probability of finding a struck proton with a large initial momentum in the ground-state wave function of the deuteron. At small  $\theta_{\text{ng}}$ , the calculated cross sections with FSI differ much less from the PWIA results and are sensitive to the type of nucleon-nucleon potential used for  $p_m > 0.45$  GeV/ $c$ , further confirming the fact that the reduced cross section in this case reflects closely the underlying momentum distribution of the deuteron.

We measured  ${}^2\text{H}(e, e'p)n$  cross sections at a momentum transfer of  $3.5(\text{GeV}/c)^2$  over a kinematical range that allowed us to study this reaction for a set of fixed missing momenta as a function of the neutron recoil angle  $\theta_{\text{ng}}$ . We experimentally confirmed the validity of the generalized eikonal approximation, which predicted a strong angular dependence of FSI contributions and kinematic regions where FSI contributions are small.

The small kinematic bin size made it possible for the first time to determine missing momentum distributions for several, fixed values of the neutron recoil angle,  $\theta_{\text{ng}}$ , and to observe a qualitative change in their shape. With decreasing  $\theta_{\text{ng}}$ , the momentum distributions change from the typical form found in previous experiments to a shape that follows more closely the trend of the deuteron wave

function in momentum space. This transition is consistent with decreasing FSI contributions and gives us for the first time a direct access to the high momentum component of the deuteron momentum distribution. We find that, within the MS model, the calculations using the CD-Bonn potential are in best agreement with the data.

We acknowledge the outstanding efforts of the staff of the Accelerator and Physics Divisions at Jefferson Lab who made this experiment possible. This work was supported in part by the Department of Energy under Contracts No. DE-FG02-99ER41065 and No. DE-AC02-06CH11357, the Italian Istituto Nazionale di Fisica Nucleare, the French Centre National de la Recherche Scientifique, and the National Science Foundation. Jefferson Science Associates (JSA) operates the Thomas Jefferson National Accelerator Facility for the U.S. Department of Energy under Contract No. DE-AC05-84ER40150.

\*Deceased

<sup>†</sup>Present address: Indiana University, Bloomington, IN 47405, USA.

<sup>‡</sup>Present address: Renaissance Technologies LLC, East Setauket, New York 11733, USA.

<sup>§</sup>Present address: Massachusetts Institute of Technology, Cambridge, MA 02139, USA.

- [1] L. C. Alexa *et al.*, *Phys. Rev. Lett.* **82**, 1374 (1999).
- [2] M. Garçon and J. W. Van Orden, *Adv. Nucl. Phys.* **26**, 293 (2002).
- [3] R. Gilman and F. Gross, *J. Phys. G* **28**, R37 (2002).
- [4] P. E. Bosted, R. G. Arnold, S. Rock, and Z. M. Szalata, *Phys. Rev. Lett.* **49**, 1380 (1982).
- [5] S. Rock *et al.*, *Phys. Rev. D* **46**, 24 (1992).
- [6] J. Arrington *et al.*, *Phys. Rev. Lett.* **82**, 2056 (1999).
- [7] O. Benhar, A. Fabrocini, S. Fantoni, V. R. Pandharipande, and I. Sick, *Phys. Rev. Lett.* **69**, 881 (1992).
- [8] L. L. Frankfurt, M. I. Strikman, D. B. Day, and M. Sargsyan, *Phys. Rev. C* **48**, 2451 (1993).
- [9] A. Bussiere *et al.*, *Nucl. Phys.* **A365**, 349 (1981).
- [10] K. I. Blomqvist *et al.*, *Phys. Lett. B* **424**, 33 (1998).
- [11] W. Boeglin *et al.*, *Phys. Rev. C* **78**, 054001 (2008).
- [12] P. E. Ulmer *et al.*, *Phys. Rev. Lett.* **89**, 062301 (2002).
- [13] M. Rvachev, F. Benmokhtar, and E. Penel-Nottaris *et al.*, *Phys. Rev. Lett.* **94**, 192302 (2005).
- [14] M. M. Sargsian, *Int. J. Mod. Phys. E* **10**, 405 (2001).
- [15] M. M. Sargsian *et al.*, *J. Phys. G* **29**, R1 (2003).
- [16] A. Bianconi, S. Jeschonnek, N. N. Nikolaev, and B. G. Zakharov, *Phys. Lett. B* **343**, 13 (1995).
- [17] L. L. Frankfurt, W. G. Greenberg, J. A. Miller, M. M. Sargsian, and M. I. Strikman, *Z. Phys. A* **352**, 97 (1995).
- [18] L. L. Frankfurt, M. M. Sargsian, and M. I. Strikman, *Phys. Rev. C* **56**, 1124 (1997).
- [19] S. Jeschonnek, *Phys. Rev. C* **63**, 034609 (2001).
- [20] C. Ciofi degli Atti and L. P. Kaptari, *Phys. Rev. Lett.* **100**, 122301 (2008).
- [21] S. Jeschonnek and J. W. Van Orden, *Phys. Rev. C* **78**, 014007 (2008).

- [22] S. Jeschonnek and J.W. Van Orden, *Phys. Rev. C* **80**, 054001 (2009).
- [23] C. Ciofi degli Atti and L.P. Kaptari, *Phys. Rev. C* **71**, 024005 (2005).
- [24] J.M. Laget, *Phys. Lett. B* **609**, 49 (2005).
- [25] S. Jeschonnek and J.W. Van Orden, *Phys. Rev. C* **81**, 014008 (2010).
- [26] M.M. Sargsian, *Phys. Rev. C* **82**, 014612 (2010).
- [27] K.S. Egiyan *et al.*, *Phys. Rev. Lett.* **98**, 262502 (2007).
- [28] John Alcorn *et al.*, *Nucl. Instrum. Methods Phys. Res., Sect. A* **522**, 294 (2004).
- [29] J. Arrington, *Phys. Rev. C* **69**, 022201(R) (2004).
- [30] V.L. Rvachev and T.I. Sheiko, *Appl. Mech. Rev.* **48**, 151 (1995).
- [31] <http://hallaweb.jlab.org/software/mceep/mceep.html> (2006).
- [32] [https://hallcweb.jlab.org/wiki/index.php/Monte\\_Carlo](https://hallcweb.jlab.org/wiki/index.php/Monte_Carlo) (2009).
- [33] R. Ent, B.W. Filippone, N.C.R. Makins, R.G. Milner, T.G. O'Neill, and D.A. Wasson, *Phys. Rev. C* **64**, 054610 (2001).
- [34] T. de Forest, *Nucl. Phys.* **A392**, 232 (1983).